

Ca_{2.5}Sr_{0.5}GaMn₂O₈: Diamagnetic Ga in Control of the Structural and Electronic Properties of a Bilayered Manganate

Peter D. Battle,^{*,†} Stephen J. Blundell,[‡] Michael L. Brooks,[‡] Maryvonne Hervieu,[§] Czeslaw Kapusta,^{||} Tom Lancaster,[‡] Santhosh P. Nair,[†] Colin J. Oates,^{||} Francis L. Pratt,[#] Matthew J. Rosseinsky,^{*,⊥} Rocío Ruiz-Bustos,[†] Marcin Sikora,^{||} and Christopher A. Steer[‡]

Contribution from the Inorganic Chemistry Laboratory, Oxford University, South Parks Road, Oxford, OX1 3QR, United Kingdom, Clarendon Laboratory, Department of Physics, Oxford University, Parks Road, Oxford, OX1 3PU, United Kingdom, Laboratoire CRISMAT, UMR 6508 associée au CNRS, ISMRa, 6 Boulevard du Maréchal Juin, 14050 Caen Cedex, France, Department of Solid State Physics, Faculty of Physics and Nuclear Techniques, AGH University of Science and Technology, Av. Mickiewicza 30-059, Cracow, Poland, ISIS Facility, Rutherford Appleton Laboratory, Chilton, Oxfordshire, OX11 0QX, United Kingdom, and Department of Chemistry, University of Liverpool, Liverpool, L69 7ZD, United Kingdom

Received June 14, 2004; E-mail: peter.battle@chem.ox.ac.uk; m.j.rosseinsky@liverpool.ac.uk

Abstract: The temperature dependence of the crystal structure and electronic properties of brownmillerite-like Ca_{2.5}Sr_{0.5}GaMn₂O₈ has been studied by neutron powder diffraction and μ SR spectroscopy. The results show that short-range 2D magnetic order begins to develop within the perovskite-like bilayers of MnO₆ octahedra approximately 50 K above the 3D Néel temperature of \sim 150 K. The bilayers show a structural response to the onset of magnetism throughout this temperature range whereas the GaO₄ layers that separate the bilayers only respond below the 3D ordering temperature. XANES spectroscopy shows that the sample contains Mn³⁺ and Mn⁴⁺ cations in a 1:1 ratio, and the behavior in the region of the Néel transition is interpreted as a local charge ordering. Electron diffraction and high-resolution electron microscopy have been used to show that the local microstructure is more complex than the average structure revealed by neutron diffraction, and that microdomains exist in which the GaO₄ tetrahedra show different orientations. It is argued that the bonding requirements of diamagnetic gallium control the electronic behavior within the perovskite-like bilayers.

Introduction

We have recently shown by neutron diffraction¹ that Ca_{2.5}Sr_{0.5}GaMn₂O₈ is an anion-deficient perovskite in which the vacant oxide sites order so as to create a structure in which perovskite bilayers consisting of MnO₆ octahedra are isolated from each other by a single layer of GaO₄ tetrahedra (Figure 1). At 5 K the material is antiferromagnetic (Figure 1c) with an ordered magnetic moment of 3.09(1) μ_B per Mn cation, the latter having a mean oxidation state of 3.5. Magnetometry and muon spin relaxation (μ SR)¹ data have shown that the transition to a magnetically ordered state occurs over a finite temperature range between \sim 150 and 125 K, and the resistivity decreases by an order of magnitude at 125 K, with \sim 50% negative magnetoresistance being observed in a field of 80 kOe at 110 K. This

compound is therefore highly relevant to the current search for new materials that might have applications in spin valves, field sensing and data storage. This quest for new materials with possible device applications has raised a number of fascinating fundamental questions concerning spin, charge, and orbital ordering in mixed-metal oxides.^{2–7} The existence of long-range ordering of the +3 and +4 oxidation states onto distinct crystallographic sites in manganates is currently controversial even at the mean oxidation state of +3.5, with more complex charge distributions over groups of Mn cations in these materials being proposed.⁶ Although there is no evidence for long-range charge ordering in Ca_{2.5}Sr_{0.5}GaMn₂O₈, we tentatively suggested, in the light of the observed bond lengths, that the ferromagnetic

[†] Inorganic Chemistry Laboratory, Oxford University.
[‡] Department of Physics, Oxford University.
[§] Laboratoire CRISMAT.
^{||} Department of Solid State Physics, Faculty of Physics and Nuclear Techniques, AGH University of Science and Technology.
[#] Rutherford Appleton Laboratory.
[⊥] Department of Chemistry, University of Liverpool.
(1) Battle, P. D.; Blundell, S. J.; Santhosh, P. N.; Rosseinsky, M. J.; Steer, C. *J. Phys.: Condensed Matter* **2002**, *14*, 13569.

(2) Radaelli, P. G.; Cox, D. E.; Capogna, L.; Cheong, S. W.; Marezio, M. *Phys. Rev. B* **1999**, *59*, 14440.
(3) Ibarra, M.; Retoux, R.; Hervieu, M.; Autret, C.; Maignan, A.; Martin, C.; Raveau, B. *J. Solid State Chem.* **2003**, *170*, 361.
(4) Hervieu, M.; Malo, S.; Perez, O.; Beran, P.; Martin, C.; Baldinozzi, G.; Raveau, B. *Chem. Mater.* **2003**, *15*, 523.
(5) Blake, G. R.; Chapon, L.; Radaelli, P. G.; Argyriou, D. N.; Gutmann, M. J.; Mitchell, J. F.; *Phys. Rev. B* **2002**, *66*, 144412.
(6) Daoud-Aladine, A.; Rodriguez-Carvajal, J.; Pinsard-Gaudart, L.; Fernandez-Diaz, M. T.; Revcolevschi, A. *Phys. Rev. Lett.* **2002**, *89*, 097205.
(7) Kimura, T.; Goto, T.; Shintani, H.; Ishizaka, K.; Arima, T.; Tokura, Y. *Nature* **2003**, *426*, 55.

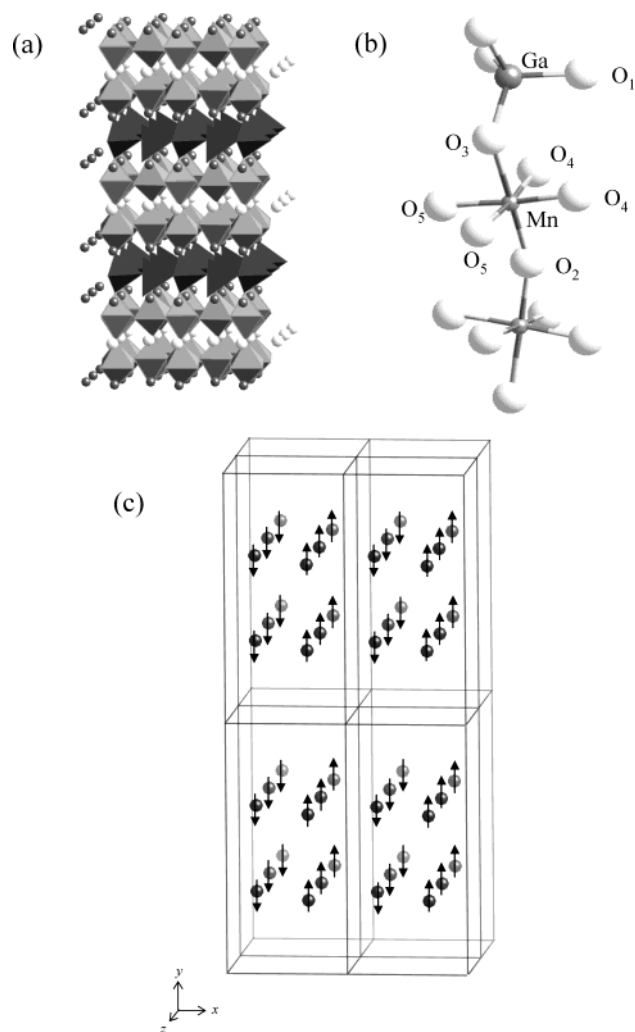


Figure 1. Structure of $\text{Ca}_{2.5}\text{Sr}_{0.5}\text{GaMn}_2\text{O}_8$: (a) polyhedral representation with MnO_6 octahedra and GaO_4 tetrahedra shaded light and dark, respectively. Light circles represent Ca/Sr cations, dark circles Ca only; (b) local coordination around the Mn and Ga sites (c) antiferromagnetic arrangement of Mn cations at 5 K, viewed perpendicular to [010].

coupling along the direction perpendicular to the perovskite layers can be attributed to a σ superexchange interaction between pairs of neighboring Mn^{3+} and Mn^{4+} cations, the half-filled e_g orbital of the former being aligned approximately parallel to this direction. The consequent presence of empty e_g orbitals and half-filled t_{2g} orbitals within the perovskite sheets then leads to antiferromagnetic coupling, in contrast to the so-called A-Type $n = 2$ Ruddlesden–Popper bilayer compounds⁸ in which ferromagnetic coupling occurs within the individual sheets as a consequence of the occupancy of the in-plane e_g orbital. We describe below an investigation of the microstructure of the compound by electron microscopy, which allows us to assess the extent to which the average bulk structure determined by X-ray and neutron diffraction is representative of the local microscopic structure, and XANES experiments designed to probe further the electronic structure of the Mn cations. We also describe the results of neutron diffraction and μSR experiments carried out at temperatures close to those of the electronic phase transitions in an attempt to clarify their nature

and identify structural changes indicative of the occurrence of charge ordering in the critical region.

Experimental Section

The polycrystalline sample used in these experiments was the same as that used in the initial characterization of this compound and preparative details have therefore been given previously.¹ To verify the mean oxidation state of Mn, XANES (X-ray absorption near edge structure) measurements were carried out. The absorption coefficient in the vicinity of the absorption edge is approximately proportional to the density of unoccupied states and the XANES spectra can therefore be regarded as fingerprints of the different valence states of an element in the solid state. The experiments were carried out on the BACH beamline facility in ELETTRA Synchrotron Laboratory in Trieste, Italy. $\text{Mn:L}_{2,3}$ XANES spectra were measured at room temperature on powder samples of $\text{Ca}_{2.5}\text{Sr}_{0.5}\text{GaMn}_2\text{O}_8$ and the reference materials Mn_2O_3 and MnO_2 by means of the total electron yield detection. Edge steps were removed from the data using arctan functions which were subtracted from the raw $\text{Mn:L}_{2,3}$ spectra, and the area under the $L_{2,3}$ edge peaks was normalized to unity for all the spectra, including Mn_2O_3 and MnO_2 which serve as references for Mn^{3+} and Mn^{4+} respectively. We thus obtained the broadened densities of unoccupied Mn 3d states. To determine the relative amount of Mn^{3+} and Mn^{4+} in $\text{Ca}_{2.5}\text{Sr}_{0.5}\text{GaMn}_2\text{O}_8$, the spectrum of that compound was fitted to a weighted sum of the Mn_2O_3 (Mn^{3+}) and MnO_2 (Mn^{4+}) spectra: $\mu(E) = x\mu_{\text{Mn}_2\text{O}_3}(E) + (1 - x)\mu_{\text{MnO}_2}(E)$.

Samples of $\text{Ca}_{2.5}\text{Sr}_{0.5}\text{GaMn}_2\text{O}_8$ were prepared for transmission electron microscopy (TEM) by crushing the crystals in butanol. The flakes in the suspension were deposited onto a holey carbon film, supported by a copper grid. The electron diffraction (ED) investigation was carried out with a 2010 JEOL electron microscope and the high-resolution electron microscopy (HREM) study with a TOPCON 002B ($V = 200$ kV, $C_s = 0.4$ mm); both microscopes were equipped with Energy Dispersive Spectroscopy (EDS) analyzers. Theoretical images were calculated for different values of focus and crystal thickness using the multi-slice method as implemented in the Mac Tempas software.

Time-of-flight neutron powder diffraction data were collected on the GEM diffractometer at ISIS, Rutherford Appleton Laboratory. The sample, of mass 4.8 g, was contained in a vanadium can of diameter 8 mm and mounted in a helium cryostat. Data were collected over the temperature range $100 \leq T/\text{K} \leq 300$ with a step size of 10 K. At most temperatures data were collected for 20 min, although a period of 1 h was used at 100, 150, and 300 K. The data from four detector banks were analyzed simultaneously by the Rietveld method⁹ using the GSAS program package.¹⁰ Our earlier work showed that the diffraction pattern of the compound $\text{Ca}_{2.5}\text{Sr}_{0.5}\text{GaMn}_2\text{O}_8$ collected at 300 K could be indexed in the orthorhombic space group $\text{Pcm}2_1$ with unit cell parameters $a = 5.4294(1)$, $b = 11.3722(3)$, and $c = 5.2983(1)$ Å which are related to the unit cell parameter, a_p , of a primitive cubic perovskite as follows: $a \sim \sqrt{2}a_p$, $b \sim 3a_p$, $c \sim \sqrt{2}a_p$. At 5 K the ordered components of the magnetic moments of the Mn cations were shown to align along [010]. In the analysis of the time-of-flight data collected at 300 K, the unit cell parameters were held at the values derived previously from constant-wavelength neutron diffraction data and the instrumental parameters (DIFC, DIFA, and ZERO) were allowed to vary. In the analysis of the time-of-flight data collected at lower temperatures, these instrumental parameters were held fixed. As previously, we used isotropic atomic displacement parameters to model thermal motion, and the z coordinate of the Mn cation was fixed to define an origin along the 2_1 -screw axis. The Sr atoms were assumed to occupy 50% of the A sites at the center of the octahedral double layer, the remainder being

(8) Battle, P. D.; Rosseinsky, M. J. *Curr. Opin. Solid State Mater. Sci.* **1999**, *4*, 163.

(9) Rietveld, H. M. *J. Appl. Crystallogr.* **1969**, *2*, 65.
(10) Larson, A. C.; von-Dreele, R. B. General Structure Analysis System (GSAS) Report LAUR 86-748 Los Alamos National Laboratories, 1990.

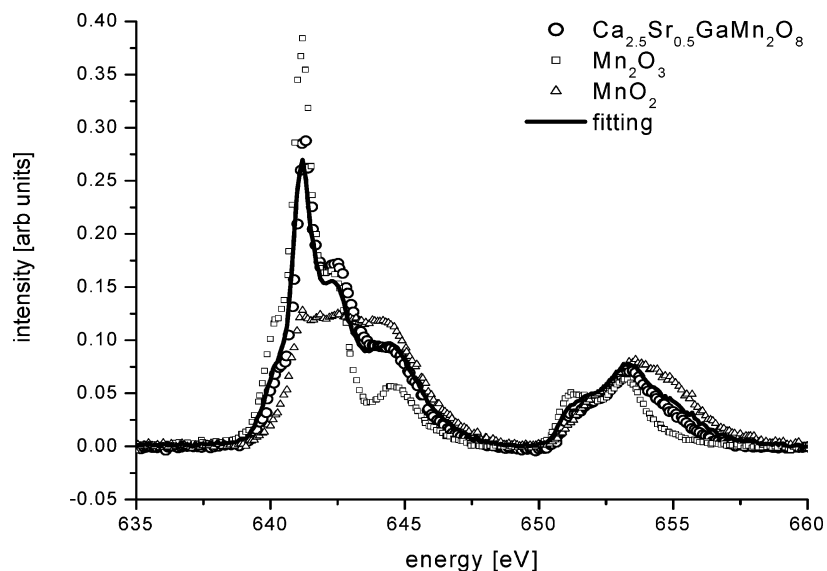


Figure 2. Mn:L_{2,3} edge XANES spectra of Ca_{2.5}Sr_{0.5}GaMn₂O₈, Mn₂O₃ and MnO₂ at room temperature. The solid line is the fit to the data, as discussed in the text.

occupied by Ca. In the final analysis of those data sets that showed magnetic Bragg scattering, the ordered moment was constrained to lie along [010].

Muon spin rotation (μ SR) data were collected on the ARGUS spectrometer at the ISIS Pulsed muon facility in the United Kingdom and on the π M3 beamline at the Paul Scherrer Institute (PSI) in Switzerland. In our μ SR experiment, spin polarized positive muons (μ^+ , momentum 28 MeV/c) were implanted into a sample of polycrystalline Ca_{2.5}Sr_{0.5}GaMn₂O₈ which had been packed in a silver foil and mounted in a ⁴He cryostat. The muons stop in the sample very quickly (in 10^{-9} s) and without significant loss of spin-polarization. The observed quantity is then the subsequent time evolution of the muon spin polarization, which can be detected by counting emitted decay positrons forward (f) and backward (b) of the initial muon spin direction; this is possible due to the asymmetric nature of the muon decay,^{11–13} which takes place in a mean time of 2.2 μ s. In our experiments positrons are detected by using scintillation counters placed in front of and behind the sample. We record the number of positrons detected by forward (N_f) and backward (N_b) counters as a function of time and calculate the asymmetry function, $G_z(t)$ using $G_z(t) = (N_f(t) - \alpha_{\text{exp}} N_b(t))/(N_f(t) + \alpha_{\text{exp}} N_b(t))$, where α_{exp} is an experimental calibration constant and differs from unity due to nonuniform detector efficiency. The quantity $G_z(t)$ is then proportional to the average spin polarization, $P_z(t)$, of muons stopping within the sample. The former quantity has a maximum value less than one since the positron decay is only preferentially, not wholly, in the direction of the muon spin. $P_z(t)$ has a maximum value of one. The muon spin precesses around a local magnetic field, B (with an angular frequency $\gamma_\mu|B|$, where $\gamma_\mu = 2\pi \times 135.5$ MHz/T).

Results

Figure 2 presents XANES spectra of Ca_{2.5}Sr_{0.5}GaMn₂O₈ and the reference samples together with a fit to the spectrum of the bilayer manganate based on a weighted sum of the reference spectra. The average Mn valence determined from the fit is 3.50(5), which corresponds to a 1:1 mixture of Mn³⁺:Mn⁴⁺ and is therefore consistent with the proposed stoichiometry of the sample and with a description based on the presence of two

distinct oxidation states for Mn. The bilayered brownmillerite material studied here is directly comparable with the perovskite and mono- and bilayered Ruddlesden–Popper phases in which the ordering of the Mn valence states onto different sites is currently controversial.¹⁴ The successful fitting of the XANES spectra to weighted sums of reference materials with the two distinct oxidation states contrasts with the analysis of the prototype CE-structured, charge-ordered material La_{0.5}Ca_{0.5}MnO₃ and indicates that electron hopping between the Mn sites in Ca_{2.5}Sr_{0.5}GaMn₂O₈ is slow on the XANES time scale of 10^{-15} s, although it should be recalled that the view of a structure offered by local spectroscopies is intrinsically different to the bulk average offered by the refinement of Bragg diffraction intensities as described below. The coherence length and existence time of charge-ordered structures may make them intrinsically difficult to detect with diffraction methods.

As a check on the homogeneity of the sample, the initial stage of the TEM characterization involved coupled ED/EDS analyses of about fifty crystallites. ED demonstrated that the sample was highly crystalline and the EDS measurements confirmed that, within the limits of the technique, the cation composition was close to the nominal one, namely Ca_{2.5}Sr_{0.5}Ga per two Mn cations. The sample was then characterized in reciprocal space by tilting around the crystallographic axes. All the ED patterns contained a set of intense reflections from an orthorhombic cell with a ≈ 5.43 Å $\approx a_p \sqrt{2}$, $b \approx 11.37$ Å $\approx 3a_p$, $c \approx 5.3$ Å $\approx a_p \sqrt{2}$, where a_p is the unit cell parameter of the primitive perovskite substructure. The systematic absences were consistent with the space group Pcm2₁, in agreement with previous results.¹ This is exemplified by the [10 $\bar{1}$] and [001] ED patterns presented in Figure 3, parts a and b, which respectively correspond to the [100]_p and [110]_p directions of the perovskite unit cell. In these patterns, the pointlike shape of the reflections attests that the periodicity $3a_p$, i.e., 11.37 Å, associated with the ordering of the MnO₆ octahedra and GaO₄ tetrahedra along the y axis is well established. However, when viewed along [100], only a few crystallites exhibit the ideal HREM image contrast and the

(11) Blundell, S. J. *Contemp. Phys.* **1999**, *40*, 175.

(12) Cox, S. F. J. *J. Phys. C* **1987**, *20*, 3187.

(13) Dalmas-de-Reotier, P.; Yaouanc, A. *J. Phys.: Condens. Matter* **1997**, *9*, 9113.

(14) Garcia, J.; Sanchez, M. C.; Subias, G.; Blasco, J. *J. Phys.: Condens. Matter* **2001**, *13*, 3229.

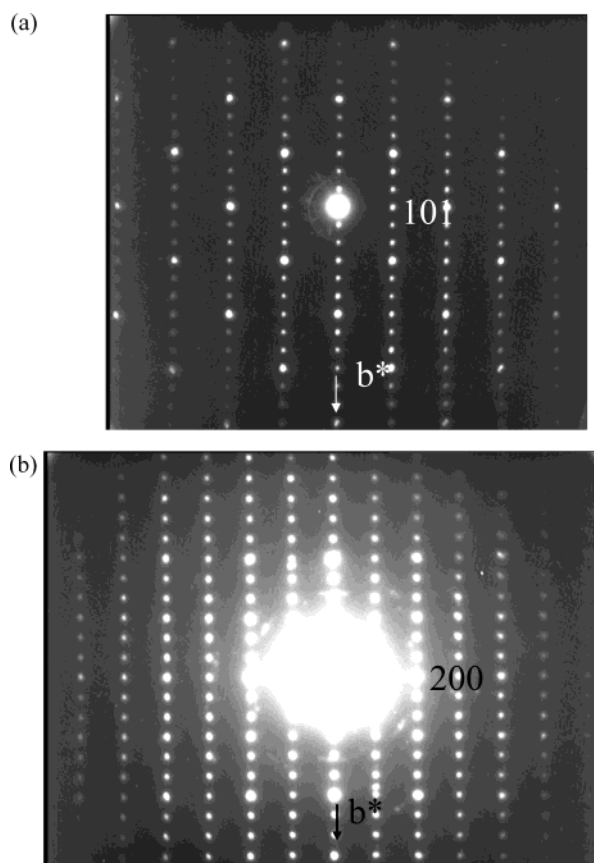


Figure 3. (a) $[10\bar{1}]$ and (b) $[001]$ ED patterns of $\text{Ca}_{2.5}\text{Sr}_{0.5}\text{GaMn}_2\text{O}_8$ at room temperature.

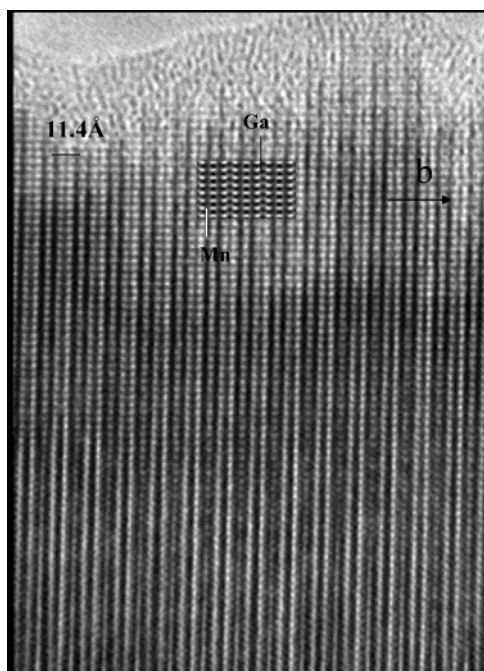


Figure 4. $[100]$ HREM image of the $\text{Pcm}2_1$ -type crystals of $\text{Ca}_{2.5}\text{Sr}_{0.5}\text{GaMn}_2\text{O}_8$, recorded for a focus value close to the Scherzer value. The theoretical image is shown in the insert.

ED patterns expected for a perfect $\text{Pcm}2_1$ -type structure, that is with the condition $0kl:l = 2n$. An example of such normal contrast is given in Figure 4. The image was recorded at a focus value $\sim -350 \text{ \AA}$, (close to the Scherzer value) where the areas

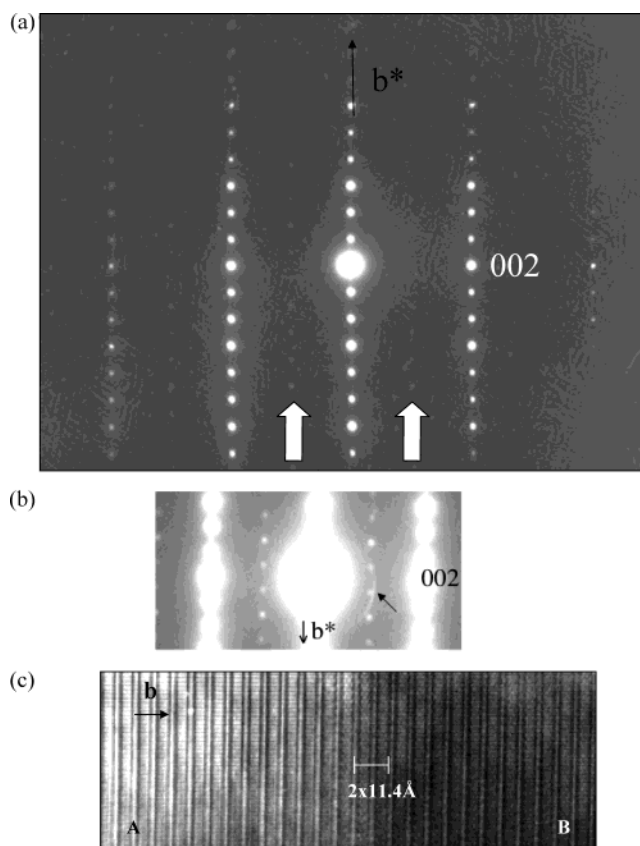


Figure 5. (a) $[100]$ ED pattern of $\text{Ca}_{2.5}\text{Sr}_{0.5}\text{GaMn}_2\text{O}_8$ exhibiting very weak additional reflections. (b) example of $[100]$ pattern with visible extra reflections and diffuse streaks along $[010]^*$. (c) $[100]$ HREM image showing two domains, the right part, labeled B, is characteristic of the centered superstructure.

of high electron density appear as the dark spots. In the thin part of the crystal, the Ga positions appear as the gray dots surrounded by two rows of bright dots. The theoretical image, calculated for the positional parameters given in ref 1 and a crystal thickness of 22 \AA , is superimposed to the experimental one. It can be seen that the agreement is good and that the contrast evolves regularly with crystal thickness in both the observed and calculated images.

Nevertheless, TEM studies of other crystallites showed that this sample of $\text{Ca}_{2.5}\text{Sr}_{0.5}\text{GaMn}_2\text{O}_8$ has a more complex microstructure, characterized by the appearance of weak extra reflections and very diffuse streaks along $[010]^*$, as can be illustrated by two examples. In Figure 5a, very weak additional reflections, scarcely visible in this $[100]$ ED pattern, can be observed: they are located at $0, k + 1/2, l$ with $l = 2n + 1$ and are indicated by the white arrows. These extra peaks violate the conditions of the $\text{Pcm}2_1$ space group and indicate a doubling of the periodicity along the y axis. The parameters of the local super-cell are $a_s \approx a_p \sqrt{2}$, $b_s \approx 2 \times 11.37 \text{ \AA} \approx 6a_p$, $c_s \approx a_p \sqrt{2}$ and it is likely to be centered with the space group $\text{Ibm}2$, as previously proposed for other similar compounds.^{15,16} The ED pattern in Figure 5b shows an area where the extra spots are more intense and the corresponding HREM image is given in

(15) Krekels, T.; Milat, O.; VanTendeloo, G.; Amelinckx, S.; Babu, T. G. N.; Wright, A. J.; Greaves, C. *J. Solid State Chem.* **1993**, *105*, 313.

(16) Vaughney, J. T.; Thiel, J. P.; Hasty, E. F.; Groenke, D. A.; Stern, C. L.; Poeppelmeier, K. R.; Dabrowski, B.; Hinks, D. G.; Mitchell, A. W. *Chem. Mater.* **1991**, *3*, 935.

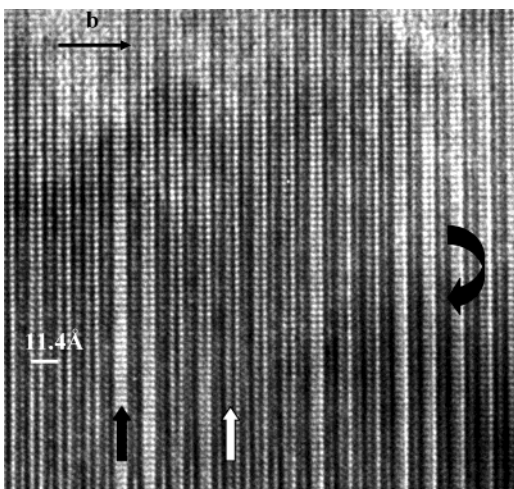


Figure 6. HREM image of Ca_{2.5}Sr_{0.5}GaMn₂O₈ showing the formation of *Ibm2*-type arrangements at the level of the [GaO] layers (black arrows) in the *Pcm2*₁-type matrix; they appear in the form of a single slice or extended areas (curved arrow).

Figure 5c, showing the coexistence of two domains, labeled A and B. In domain A, the periodicity along *y* is 11.37 Å, and 2.7 Å along the perpendicular direction, consistent with the [100] images of the *Pcm2*₁-type structure, whereas in domain B, the centered contrast is consistent with the [100] projection of an *Ibm2*-type structure.

In Figure 6, recorded at the same focus value, the periodicity is 11.37 Å × 2.7 Å over the whole area. However, variations in the contrast are clearly observed at the locations of the [GaO] layers, as indicated by the straight black and white arrows. The contrast at the rows indicated by white arrows, i.e., one row of gray dots sandwiched between two rows of bright dots, is the experimental one observed for the [100] images of the *Pcm2*₁-type structure (see Figure 4), whereas the black arrows indicate regions where the contrast is different and appears brighter since the gray dots are not visible. This phenomenon is observed either in the form of an isolated event in the normal matrix, or in the form of larger areas, as observed in the right-hand side of the image (see curved arrow). The EDS analyses could not detect a significant deviation of the cationic composition between these parts of the crystallites. This suggests that the phenomenon is related to the arrangement of the tetrahedra that can adopt two orientations in zigzag chains at the level of the [GaO] layers. Preliminary calculations carried out with an ideal model of an *Ibm2*-type structure show that the experimental contrast is in agreement with this hypothesis. The existence of both local and extended defects in the nonmagnetic layers connecting the manganate bilayers is an important aspect of the structure to consider when interpreting the evolution of the magnetic properties.

All of the neutron diffraction data could be accounted for in the space group *Pcm2*₁; there was evidence for neither a doubling of the unit cell volume nor a change of space group on cooling. The absence of a detectable change in space group symmetry means there is no crystallographic evidence for localization of distinct manganese oxidation states on different sites—any such changes (taking place, for example, on a length scale too short to be detected by neutron diffraction) are thus necessarily averaged over the space group symmetry operators used here. Figure 7 shows that the in-plane unit cell parameters

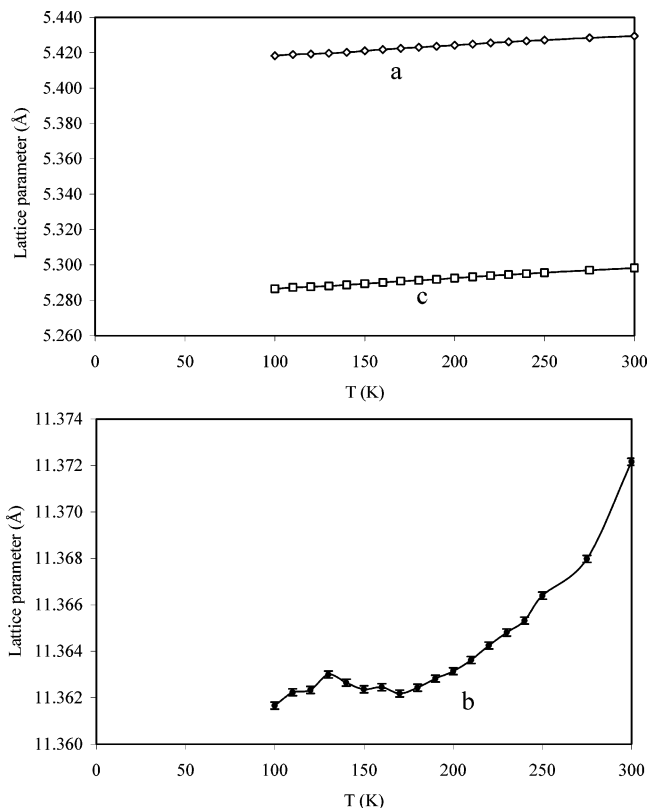


Figure 7. Temperature dependence of the unit cell parameters of Ca_{2.5}Sr_{0.5}GaMn₂O₈.

a and *c* decrease smoothly on cooling, whereas *b*, describing the period along the axis perpendicular to the perovskite layers and parallel to the ordered magnetic moment, decreases on cooling from 300 to 170 K, increases slightly on cooling from 170 to 130 K and then decreases again on further cooling; the unit cell volume decreases on cooling throughout the temperature range of the measurements. Figure 8 shows the evolution on cooling from 300 K of the scattering at a *d* spacing of ~5.5 Å. Magnetic scattering is scarcely apparent in the data collected at 200 K, but diffuse scattering is clearly visible at 170 K, and at 140 K a Bragg peak is present. The diffuse scattering is only visible for the 100 and 001 reflection positions, consistent with short-range order correlated within, but not between, the bilayer perovskite blocks. However, there was no well-defined transition between scattering that must be classified as diffuse, and therefore attributable to short range order, and scattering that forms obvious Bragg peaks as a consequence of long-range magnetic order. Figure 9 shows the result of attempting to refine an ordered Mn magnetic moment at each temperature. This quantitative analysis shows that nonnuclear scattering is present at and below 200 K, and the magnitude of this scattering grows rapidly below 150 K; the value of the magnetic moment plotted at 5 K is that determined in our earlier study of this compound. These data lead us to conclude that significant short-range magnetic order is present in the temperature range 150 ≤ *T*/K ≤ 200, and that the transition to a long-range ordered state occurs close to 150 K. Although it is clear from the behavior of the unit cell parameter *b* (Figure 7) that the crystal structure responds to the onset of magnetic ordering, attempts to correlate the magnetic behavior with the interatomic distances in the crystal structure are limited by the precision of our results; the

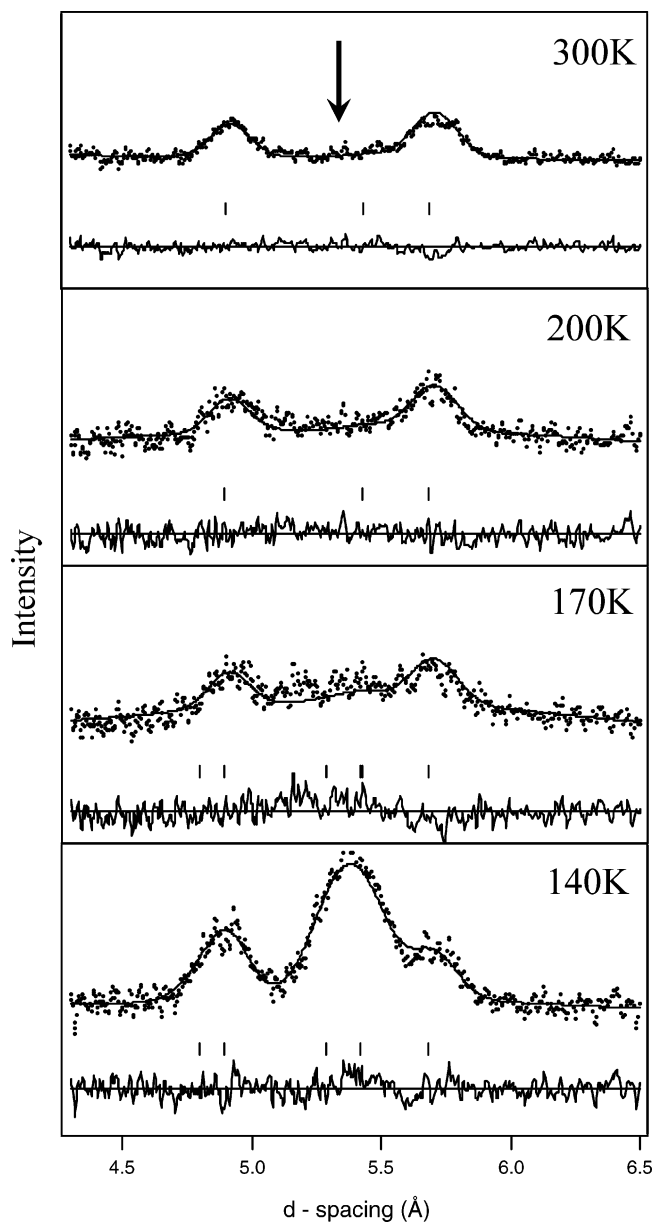


Figure 8. Temperature dependence of the observed (\bullet) and calculated ($-$) neutron diffraction profiles of $\text{Ca}_{2.5}\text{Sr}_{0.5}\text{GaMn}_2\text{O}_8$, together with a difference curve; a region of increasing magnetic scattering, corresponding to the 100 and 001 Bragg reflection positions, is arrowed.

changes in the individual bond lengths and angles are less well defined than the changes in the unit cell parameter which is effectively their resultant. The extent of electron localization in manganates is often considered in terms of the extent of Jahn–Teller distortion at the Mn sites—this does not change between 100 K and 300 K as estimated from the standard deviation of the Mn–O distances from the mean value. However, Figure 10a provides evidence that the Mn–O2 bond, linking the two Mn sheets within the bilayer (Figure 1b), increases at the Néel temperature, whereas the trans Mn–O3 bond, linking the bilayers with the bridging but nonmagnetic Ga–O layer, does not. This distance does however decrease in the 200–150 K range, above the three-dimensional ordering temperature, where there is evidence for short-range ordering. Figure 10b shows that this asymmetric expansion is accommodated by a decrease of the Mn–O2–Mn bond angle that

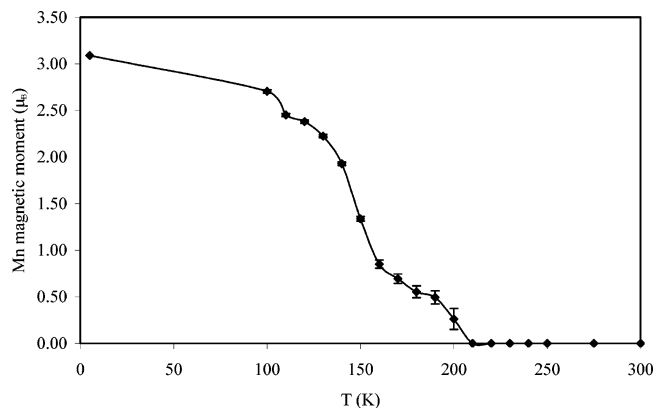


Figure 9. Temperature dependence of the ordered magnetic moment of Mn in $\text{Ca}_{2.5}\text{Sr}_{0.5}\text{GaMn}_2\text{O}_8$.

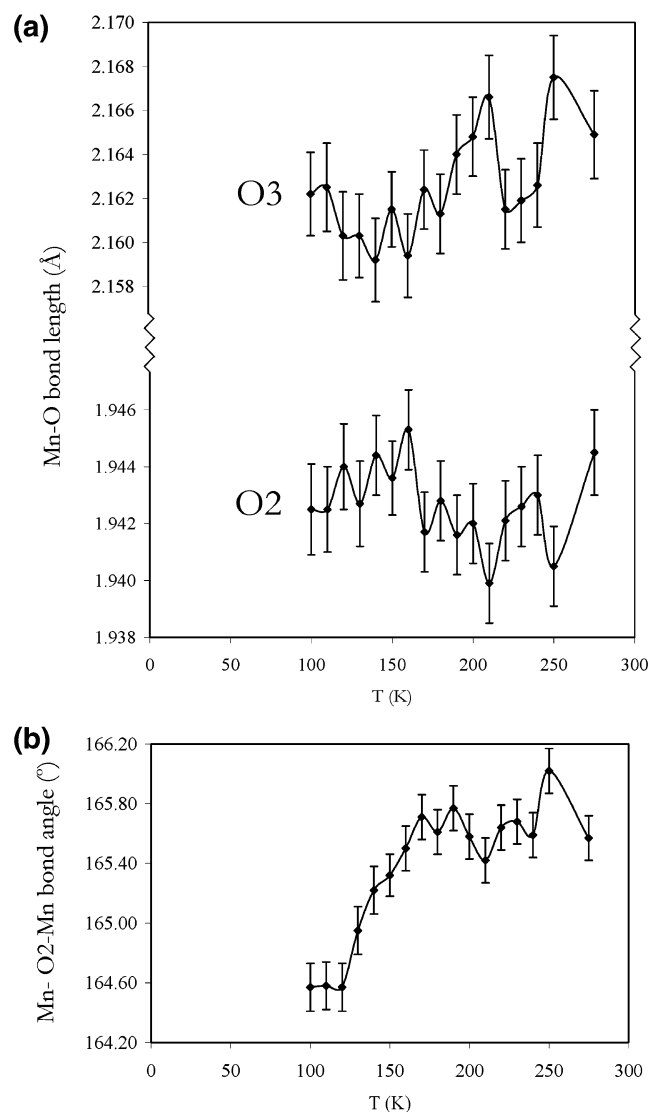


Figure 10. Temperature dependence of (a) axial Mn–O2 and Mn–O3 bond lengths and (b) Mn–O2–Mn bond angle in $\text{Ca}_{2.5}\text{Sr}_{0.5}\text{GaMn}_2\text{O}_8$.

occurs over the temperature range $170 \leq T/\text{K} \leq 130$. Figure 11a shows that both the Mn–O4 bonds within the perovskite layers shorten as the magnetic ordering develops and Figure 11b that the Mn–O5 bonds lengthen. This response corresponds to the two initially longer in-plane bonds shortening to come closer in length to the initially shorter bonds. This reduces the

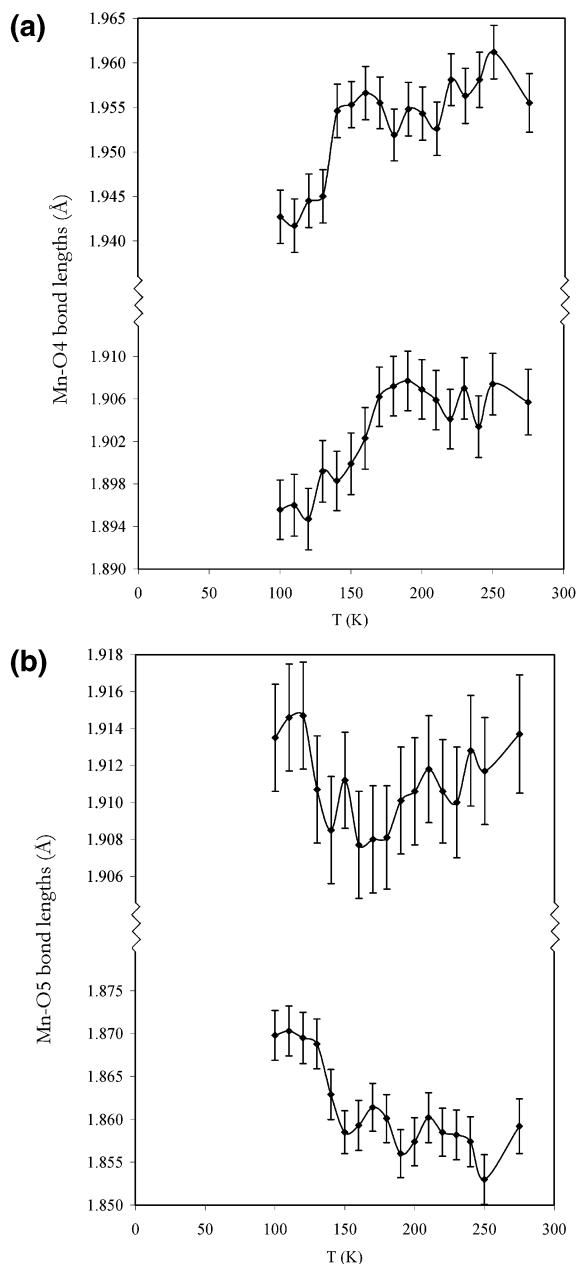


Figure 11. Temperature dependence of in-plane (a) Mn–O4 and (b) Mn–O5 bond lengths in Ca_{2.5}Sr_{0.5}GaMn₂O₈.

asymmetry of the in-plane environment at each Mn site, quantified by a decrease in the standard deviation from the mean value of the in-plane bond lengths from 0.038 Å to 0.031 Å. The environment of the gallium evolves in a surprising way (Figure 12) through the electronic transition. The largest response is apparent in the Ga–O1 distances, which is remarkable as neither atom is directly bonded to the electronically active manganese site. The two crystallographically distinct Ga–O1 distances are very similar above the transition, but below 160 K diverge in length; the Ga–O1 bond that lies above the shorter Mn–O5 distance in the neighboring manganese bilayer lengthens very slightly, whereas the other Ga–O1 distance decreases dramatically in length by almost 0.02 Å. (Figure 13) The Ga–O3 bond that links the layer of tetrahedra to the perovskite double layer does not change length (Figure 12). It is clear that the crystal structure of Ca_{2.5}Sr_{0.5}GaMn₂O₈ responds

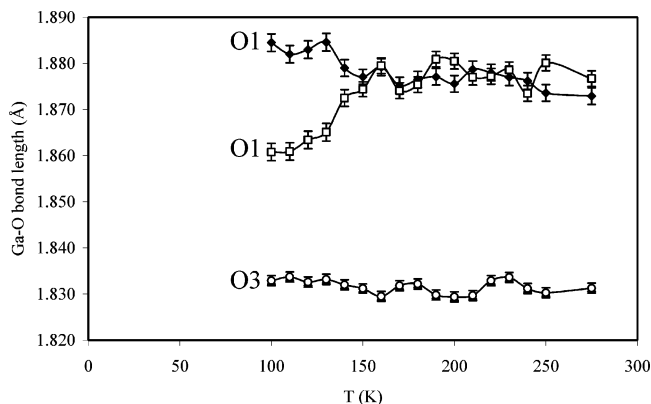


Figure 12. Temperature dependence of Ga–O bond lengths in Ca_{2.5}Sr_{0.5}GaMn₂O₈. The Ga–O1 bonds are in the GaO layer; the Ga–O3 bond connects the manganese and gallium sites.

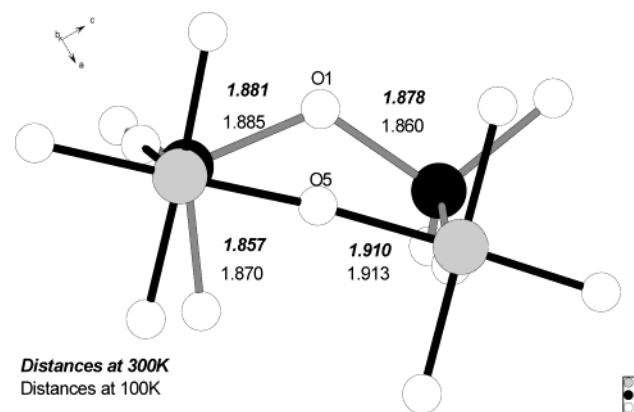


Figure 13. Mn–O5 and Ga–O1 bond configurations and their temperature dependence.

to the development of magnetic ordering; the origin of the response will be discussed below.

A preliminary account of our μ SR data taken on the ARGUS spectrometer has been presented elsewhere.¹ These data showed that the initial asymmetry of the decay positrons begins to fall due to the development of a static field below ~ 150 K. The initial asymmetry only reached its minimum near 125 K, suggesting that the entire volume of the sample is only ordered below ~ 125 K.¹ The frequency resolution of data from a pulsed muon spectrometer, such as ARGUS, is however limited because of the ~ 70 ns pulse width of the incoming muons, and precession in the internal field of a magnetic state is therefore impossible to observe if the internal field at the muon site is larger than ~ 0.05 T, which is usually the case in magnetically ordered oxides. This can make the precise determination of critical temperatures problematic since a decrease in initial asymmetry occurs as the characteristic frequency of the (often heavily damped) oscillations crosses the frequency cutoff of the spectrometer.

We therefore carried out an experiment using the GPS spectrometer at PSI, a continuous muon facility that does not suffer from the problem of limited frequency resolution, collecting data between 5 and 150 K. The raw muon asymmetry data are presented in Figure 14(a) and show clear oscillations of the muon polarization, corresponding to muon-spin precession in a quasi-static magnetic field at the muon site. The frequency of the oscillations reduces as the sample is warmed, corresponding to a reduction in the internal field. The damping of

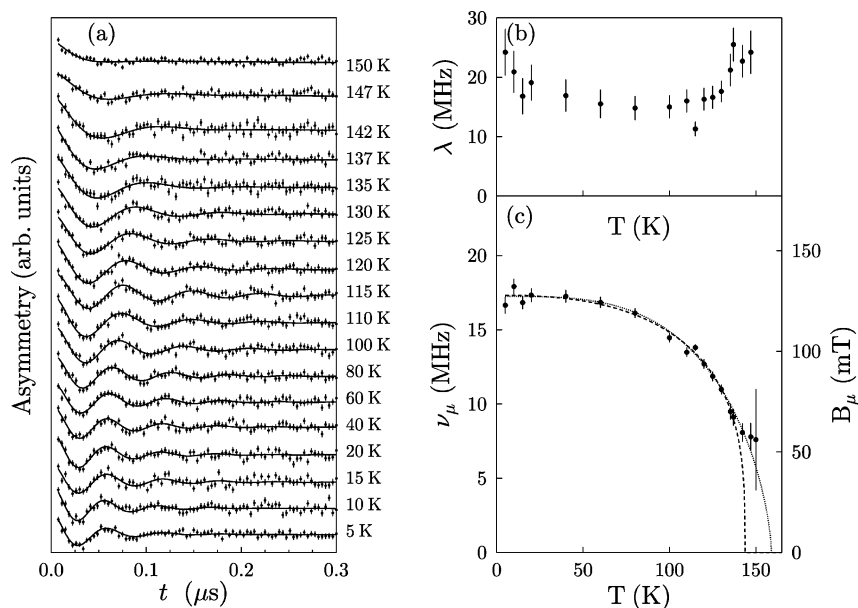


Figure 14. (a) Raw muon asymmetry data showing clear oscillations of the muon polarization, corresponding to a quasi-static magnetic field at the muon site. The data have been vertically offset from one another for clarity. (b) The temperature dependence of the damping rate λ . (c) The temperature dependence of the muon precession frequency ν_μ (and equivalently the internal magnetic field $B_\mu = 2\pi\nu_\mu/\gamma_\mu$). The dashed and dotted lines show a phenomenological fit to the temperature dependence of the internal field, fitting all data below either 140 K (dashed) or 150 K (dotted).

the oscillations increases markedly above ~ 140 K and for the trace at 150 K it is very difficult to discern a muon precession signal by eye. In this case, the data are best described by a simple nonoscillatory relaxation. The data over the entire temperature range were nevertheless fitted to a form $G_z(t) = A_1 \cos(2\pi\nu_\mu t) e^{-\lambda t} + A_2$, where A_2 represents a background contribution. The temperature dependence of the extracted values of the damping rate λ and the muon precession frequency ν_μ are shown in Figure 14, parts b and 14c, respectively. These show quite clearly that the muon precession frequency decreases as the sample is warmed. It is very difficult to extract reliably the muon precession frequency above 140 K and almost impossible at 150 K (note the large error bar on the fitted frequency for 150 K, indicative of a failure to describe adequately the data using this functional form). Consequently, the best description of these data can be found by fitting the data below 140 K to a phenomenological form $\nu_\mu(T) = (1 - (T/T_N)^\alpha)^\beta$, and we conclude that the sample shows long-range magnetic order in this region. Between 140 and 150 K the state of the sample is more uncertain, but it appears to be undergoing a crossover from uniform long-range order at 140 K and below (consistent with the Bragg peak observed at 140 K) to at most short-range order at 150 K and above. μ SR is a volume technique and so is not sensitive to minority impurity phases (in contrast to SQUID magnetometry) but is dominated by the majority volume fraction in the sample. Therefore this smooth transition is a feature of the sample as a whole, and is in stark contrast to the behavior observed in materials with a conventional, sharp magnetic transition in which $\nu_\mu(T) \rightarrow 0$ as $T \rightarrow T_N$ or T_c (see, e.g., ref 17). We note that even at low temperature, the precession signal is strongly exponentially damped (attempts to fit the data using a Gaussian damping were not successful). This indicates magnetic dynamics even at low temperatures. Curiously, the oscillations show their minimum damping rate

at intermediate temperatures (it is expected that the damping rate should rise close to T_N , but not that they should increase as the sample is cooled to 5 K). For temperatures above 150 K, the data can be fitted using a simple exponential relaxation and the temperature dependence of the relaxation rate is shown in Figure S1. The relaxation rate is only weakly temperature dependent, and rises as the sample is cooled toward 150 K as expected for critical slowing down of the spin fluctuations. At the highest temperature, we estimate the spin fluctuation rate of the Mn moments to be in the range 10–100 GHz.

Discussion

The data described above suggest that the electronic properties of $\text{Ca}_{2.5}\text{Sr}_{0.5}\text{GaMn}_2\text{O}_8$ change slowly over a wide temperature range, rather than abruptly at a single, well-defined transition temperature, and that the crystal structure undergoes subtle but significant changes in order to accommodate the electronic changes. The temperature dependence of the magnetic susceptibility¹ does not show Curie–Weiss behavior below 300 K and the μ SR data presented in Figure 14 also suggest that the transition to a long-range ordered state occurs over a wide temperature interval, in marked contrast to the behavior of the single layer brownmillerite CaSrGaMnO_5 .¹⁸ The transition is clearly preceded by the formation of regions in which extensive short-range magnetic ordering is present, presumably within the perovskite double layers which are isolated from each other by the layers of GaO_4 tetrahedra in the $\text{Ca}_{2.5}\text{Sr}_{0.5}\text{GaMn}_2\text{O}_8$ structure. This short-range order is apparent (Figure 9) in the high d spacing portion of the neutron diffraction pattern at temperatures below 200 K, although the μ SR data show that static (on a μ s time scale), long-range magnetic order is not present above 150 K. However, the observation of diffuse magnetic neutron scattering in the temperature range $150 < T/\text{K} < 200$ shows

(17) Blundell, S. J.; Pattenden, P. A.; Pratt, F. L.; Valladares, R. M.; Sugano, T.; Hayes, W. *Europhys. Lett.* **1995**, *31*, 573.

(18) Battle, P. D.; Bell, A. M. T.; Blundell, S. J.; Coldea, A. I.; Gallon, D. J.; Pratt, F. L.; Rosseinsky, M. J.; Steer, C. A. *J. Solid State Chem.* **2002**, *167*, 188.

that short-range correlations, static on a time scale of 1 ps, do exist. Fitting a Bragg peak to the enhanced neutron scattering in this temperature range is not strictly valid, but it does provide a simple quantitative indication of the degree of magnetic scattering. The lower onset temperature of the oscillations in the μ SR data is a consequence of the relatively slow time scale of the spectroscopic technique. The unusual temperature dependence of the relaxation behavior in the ordered state and the broad range over which the transition to three-dimensional order takes place might be attributable to the existence, consistent with the presence of extended defects within the intervening GaO layers, of a range of coupling pathways between the electronically active manganate bilayer blocks due to local variations in the ordering of the GaO₄ tetrahedra. The Ga–O distances clearly undergo significant changes when 3D order is established (the evolution of Ga–O1(1) being particularly marked), and these changes, coupled to the variations in orientation of the tetrahedra revealed by HRTEM, will produce a range of interaction strengths in the coupling between manganate bilayers separated by the differently arranged tetrahedral layers.

It is clear from a more detailed consideration of the bond length and unit cell data that some parameters, for example the bond angle Mn–O2–Mn, change gradually over the full width of the temperature window $120 \leq T/K \leq 200$, whereas others only change at lower temperatures, for example the bond length Ga–O1 only changes below 150 K. The development of three-dimensional long-range magnetic order requires that the superexchange between the manganate bilayers is propagated via the diamagnetic Ga–O layer, and the involvement of the Ga 3d and 4s orbitals in this pathway produces relaxation of the environment around Ga, presumably to maximize the exchange interactions.

It is not obvious how these observable changes relate to the ordering of specific Mn *d* orbitals. The absence of a center of symmetry at the Mn site allows strong *p/d* mixing, and an interpretation in terms of pure *d* orbitals can only be an approximation. The structural and electronic behavior of manganates is generally controlled by the spatial distribution of the electrons in the *e_g* orbitals associated with Mn³⁺ centers. In the present case, the small size and associated strong covalency associated with Ga³⁺ produces some important and interesting differences with previously studied compositions. The Ga–O distances are all shorter and the bonds thus stronger than the Mn–O distances. In competing with the interlayer O3 anion for bonding, the short Ga–O3 distance renders the Mn–O3 distance the longest in the structure at all temperatures and thus exerts a pinning effect on the electronic structure at each Mn site, ensuring that the 3y²-r² orbital at each Mn³⁺ site is the lower in energy of the two *e_g* orbitals. This influence of the Ga–O covalency orders the *e_g* electron at Mn³⁺ sites into the 3y²-r² orbital, making the two axially orientated Mn–O bonds the longest bonds in the structure. This conclusion, reinforced by the absence of a significant change in the ratio between in- and out-of-plane bond lengths over the temperature range studied, suggests that at all temperatures the occupied *e_g* orbitals at the Mn³⁺ centers are ordered along *y*. This is in clear contrast with the *n* = 2 RP phases Ln_{2–2*x*}Sr_{1+2*x*}Mn₂O₇ where the orbital ordering can occur along both inter- (*x* < 0.5) and intralayer (*x* > 0.5) directions, with the A- and CE-type structures driven

by ordering of x²-y² and 3y²-r² orbitals, respectively, in the MnO₂ plane.^{19–22} In the brownmillerite case, the requirements of the Ga–O bonding remove the orientational flexibility of the Mn *e_g* orbitals. The electronic structure of the material is thus controlled by the occupation of the 3y²-r² orbitals at all the temperatures studied here. The elongation of the distance Mn–O2 indicates an increase in charge density along [010] in the middle of the perovskite blocks. We can then hypothesize that on cooling, a single *e_g* electron is localized between each pair of Mn cations which share a common oxide ion (O2) along a direction close to [010], and that it is this increase in electron density that elongates the mean Mn–O2 bond length. We are thus suggesting that some form of local or dynamic charge ordering occurs, generating species that resemble the Zener polarons proposed in discussing static charge order in perovskite manganates.⁶ These dynamic correlations between the +3 and +4 valence states along *y* avoid the unfavorable situation of the O2 anion being shared by two Mn³⁺ cations with Jahn–Teller elongation along *y*—this emphasizes the difference from perovskite and RP systems where the Jahn–Teller orbitals at Mn³⁺ sites can be orthogonal.

The magnetic coupling between the pair of Mn³⁺, Mn⁴⁺ cations thus created would be expected to be ferromagnetic, as is observed experimentally. As crystallographically distinct Mn sites are not created, the valence states continue to fluctuate and although 3+/4+ correlations predominate at sites separated by O2, the reduction of the O2–Mn–O2 bond angle will increase the strength of ferromagnetic coupling in the case when sites separated by O2 are both occupied by Mn³⁺ species by reducing the overlap integral between 3y²-r² orbitals on neighboring sites and thus enhancing the ferromagnetic orthogonal orbital contribution to the superexchange. This dynamical 3+/4+ correlation will favor ferromagnetic exchange between the two MnO₂ sheets within each bilayer. The empty in-plane *e_g* orbitals do not favor any particular charge ordering scheme within the MnO₂ layers (as the x²-z² orbital at both 3+ and 4+ sites is empty, there is no elastic driving force to correlate the charges), and so the in-plane exchange interactions are antiferromagnetic and dominated by the half-filled-half-filled t_{2g} and empty-empty *e_g* correlations, both of which are antiferromagnetic. The pinning of the occupied *e_g* orbitals along the *z* direction thus gives rise to quite different magnetic structures from those found for *n* = 2 Ruddlesden–Popper and perovskite manganates.

Unlike the perovskite and RP examples with the mean Mn +3.5 oxidation state, we see no evidence for long-range, 3-dimensional ordering of the valences on different crystallographic sites despite confirming the existence at room temperature of valence states distinguishable on the XANES time scale. We have argued above that short coherence length ordering, or the development of two sites with very similar bond lengths, would not be detectable in this study. The absence of 3-dimensional long-range static charge ordering is also consistent with the enhanced conductivity, attributable to local double

- (19) Argyriou, D. N.; Bordallo, H. N.; Campbell, B. J.; Cheetham, A. K.; Cox, D. E.; Gardner, J. S.; Hanif, K.; Santos, A. d.; Strouse, G. F. *Phys. Rev. B* **2000**, *61*, 15269.
- (20) Ling, C. D.; Millburn, J. E.; Mitchell, J. F.; Argyriou, D. N.; Linton, J.; Bordallo, H. N. *Phys. Rev. B* **2000**, *62*, 15096.
- (21) Kubota, M.; Yoshizawa, H.; Morimoto, Y.; Fujioka, H.; Hirota, K.; Endoh, Y. *J. Phys. Soc. Jpn.* **1999**, *68*, 2202.
- (22) Mitchell, J. F.; Argyriou, D. N.; Berger, A.; Grey, K. E.; Osborn, R.; Welp, U. *J. Phys. Chem. B* **2001**, *105*, 10731.

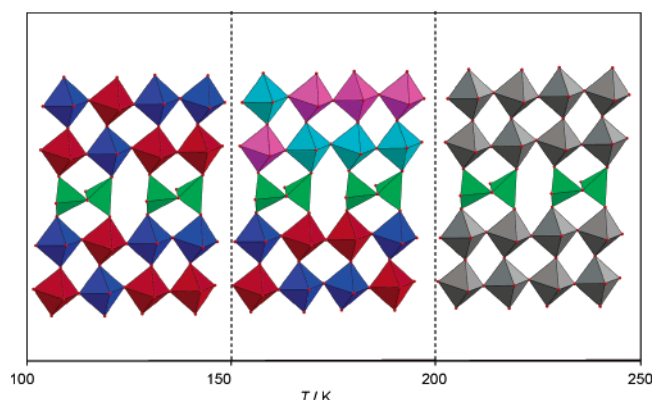


Figure 15. Schematic representation of dynamical ordering of $3y^2-r^2$ orbitals and Mn^{3+} centers. Above 200 K there is no correlation of charge at neighboring sites in the structure. Below 200 K alternation of 3+ and 4+ states as pairs along the y axis within a bilayer develops, producing magnetic correlations within the bilayers, but without orbital or spin correlations between the bilayers (represented as different colorings of pairs of octahedra within the two bilayers shown). Below 150 K the correlations extend across the bilayers via the diamagnetic GaO_4 layer to produce three-dimensional magnetic order and dynamical charge correlation.

exchange, observed in the magnetically ordered state. However, the material remains insulating at all temperatures. Figure 15 illustrates our model for the charge ordering in $\text{Ca}_{2.5}\text{Sr}_{0.5}\text{GaMn}_2\text{O}_8$. The sections of Figure 15 that provide a schematic representation of the behavior for $T > 150$ K are consistent with the arguments presented above. The representation of the behavior below 150 K has a speculative component in that we show an inter-block correlation of the orbital ordering along the y axis (a strict alternation of red and blue octahedra in each [010] chain). We are thus proposing the existence of 1-dimensional charge ordering in this direction. This alternation of Mn^{3+} and Mn^{4+} cations would be consistent with the ferromagnetic coupling observed along y and, being 1-dimensional, it would not be detected in our diffraction experiments. Transport and scattering measurements on single crystals are needed in order to confirm or refute this hypothesis, for which there is at present no direct experimental evidence.

It is clear from the data above that these changes begin at temperatures well above those at which long-range magnetic order is detected by neutron diffraction and μSR , and we propose that the structural changes initially lead to short-range 2D magnetic ordering, identified in the susceptibility data¹ and by the onset of non-Bragg neutron scattering, within the individual double layers and that 3D ordering follows at a lower temperature, close to 150 K. This corresponds to the development of orbital ordering correlated within the bilayers across the O2 anions (150–200 K) and between the bilayers via the GaO_4 tetrahedra below 150 K. This is consistent with the essential role of the GaO vacancy-containing layer in transmitting magnetic correlations between the manganate bilayers to generate three-dimensional ordering, the electronic role of this layer which formally contains no unpaired spins being clearly demonstrated by the marked structural response. The bond-valence sum around the Ga site does not change during the transition (300 K, 2.874; 100 K, 2.875) suggesting that the rearrangements of the bond lengths are all coupled to maintain the Ga valence, that is if one of the displacements is driven by electronic rearrangements at the Mn site, then all the other rearrangements will follow. The most obvious response at the

Ga site is the development of two different Ga–O1 distances within the tetrahedral layer, although O1 is not bonded to Mn. The dramatic shortening of one of these distances produces a pattern of short (Ga–O1′) and long Ga–O1 (Ga–O1′′) distances that matches in antiphase the short and long Mn–O5 distances in the neighboring MnO_2 layers (Figure 13). The three longest Ga–O distances (2 Ga–O3, 1 Ga–O1′′) lengthen by a total of 0.016 Å between 300 K and 100 K to accommodate the dramatic shortening of Ga–O1′. This correlates with the shortening of Mn–O3 between 200 K and 150 K above the three-dimensional ordering transition and occurs to produce a more regular environment around Ga, as judged from small reductions in the standard deviations of both bond lengths and angles from the mean values between 300 K and 100 K.

The dramatic shortening in Ga–O1 and divergence between Ga–O1′ and Ga–O1′′ below the three-dimensional magnetic ordering temperature thus needs to be seen in the context of the cumulative lengthening of the other three Ga–O bonds, which we suggest are coupled to the evolution of the electronic structure in the manganate bilayer—in particular the large net changes in the structure along the interlayer direction signaled by the anomalous thermal variation of the unit cell parameter *b* and the behavior of the Mn–O3 bond linking the Mn and Ga layers indicate that this is the case. The strong variations of the in-plane Mn–O4/O5 and Ga–O1 distances do not produce anomalies in the corresponding cell parameters but occur in a manner coupled to the anomalies in *b* driven by variations in the bond lengths and angles along the interlayer direction. The extent to which the nonmagnetic Ga site reorganizes to accommodate the changes in the perovskite block is remarkable, and the ability of the directional covalent bonding around the d^{10} cation to adapt in this way may be crucial to the properties of this compound. The changes in the lengths of the bonds between Ga and O1, which is not even bonded to a Mn cation, are particularly striking; we are not aware of any other manganate where ordering in the Mn-containing perovskite blocks has such marked consequences in the separating layer. The chemical contrast with the other bilayered manganates in the Ruddlesden–Popper series is that the ionic bonding to the lanthanide and alkaline earth cations in the intervening rock-salt layers is less directional and plays little role in influencing the thermal evolution of structural details (such as the preferred orbital ordering directions) in the manganate parts of the structure. In the bilayered brownmillerites, the strong covalent bonding in the tetrahedral layer requires any structural modifications in the manganate layer to be accommodated within the tetrahedral layer directly. The re-adoption by the unit cell parameter *b* of a positive expansion coefficient on cooling below 130 K is perhaps the clearest indication of the low-temperature boundary of the structural changes and the reduction in the resistivity of the material by 2 orders of magnitude thus occurs as the magnetostrictive changes reach completion, with both the ordered magnetic moment measured by neutron diffraction and the internal field measured by μSR showing small anomalies in this same temperature region (110–120 K). The results described above thus provide evidence to support the hypotheses put forward in our previous publication¹ to account for the properties of $\text{Ca}_{2.5}\text{Sr}_{0.5}\text{GaMn}_2\text{O}_8$.

However, although we have been able to offer explanations for the electronic properties of this compound in terms of the

crystal structure, it is clear that the average structure determined by neutron diffraction is not a complete description of this phase. The observation by electron microscopy of 1b2-type arrangements in the Pcm2₁-type matrix can be interpreted as a disorder phenomenon at the level of the [GaO] layers. This will give rise to a range of interlayer couplings and can be associated with the evolution of the magnetic correlations over a wide temperature range. It will thus be important to investigate in the future how the microstructure of the compound changes to accommodate the onset of magnetic ordering, and to what extent the density of intergrowths determines the electronic properties of the composition. It will also be important to pursue alternative synthesis methods in order to isolate materials in which the local structural motifs identified extend over the entire structure. In view of the close relationship between the electronic behavior of the manganate blocks and the detailed structure of the charge-balancing GaO layer due to the coupling of structural changes driven by the manganese e_g orbitals to the strong covalent

bonding at gallium, this promises the identification of new electronic states.

Acknowledgment. R.R.B. and C.J.O. acknowledge the financial support provided through the Human Potential Program of the European Community under contract HPRN-CT-2002-00293, [SCOOTMO]. Part of this work was performed at the Swiss Muon Source at the Paul Scherrer Institute, Villigen, Switzerland. We also acknowledge funding from EPSRC and experimental assistance from the staff of the ISIS and PSI facilities. The Cracow group acknowledges support from the State Committee for Scientific Research and would like to thank Dr. F. Bondino for her assistance during synchrotron measurements.

Supporting Information Available: Muon relaxation rate measured above 150 K in Ca_{2.5}Sr_{0.5}GaMn₂O₈ (Figure S1). This material is available free of charge via the Internet at <http://pubs.acs.org>.

JA0465000